Corneal Strain Induced by Intracorneal Ring Segment Implantation Visualized With Optical Coherence Elastography

Originally published in:
Journal of Refractive Surgery 38(3), https://doi.org/10.3928/1081597X-20211214-01

Funding acknowledgement:
174113 - Measuring local corneal biomechanical properties by multi-frequency vibrography: Moving towards an earlier diagnosis of pathologies and personalized computer simulations (SNF)

Corneal strain induced by intrastromal ring segment implantation visualized with optical coherence elastography

Emilio A. Torres-Netto[1,2,3,4], MD, PhD, Sabine Kling[5], PhD

[1] Laboratory of Ocular Cell Biology, Center for Applied Biotechnology and Molecular Medicine, University of Zurich, Zurich, Switzerland

[2] Faculty of Medicine, University of Geneva, Geneva, Switzerland

[3] Department of Ophthalmology, Paulista School of Medicine, Federal University of Sao Paulo, Sao Paulo, Brazil

[4] Department of Ophthalmology, University Hospital Zurich, University of Zurich, Zurich, Switzerland

[5] OPTIC team, Computer Vision Laboratory, ETH Zurich, Switzerland

Word count: 2365

Corresponding author:

Sabine Kling, OPTIC-team, Computer Vision Laboratory, Department of Information Technology and Electrical Engineering, ETH Zurich, Sternwartstrasse 7, 8092 Zurich, Switzerland, klings@ee.ethz.ch

Financial disclosure:

SK (none), ET (none)

Abstract:

Purpose: To record the axial strain field in the cornea directly after creating a stromal tunnel and implanting an intracorneal ring segment (ICRS).

Methods: Freshly enucleated porcine eyes were obtained and assigned either to ICRS implantation, tunnel creation only or virgin control. Immediately after manual tunnel creation and ICRS positioning, the entire eye globe was mounted on a customized holder and intraocular pressure (IOP) was adjusted to 15 mmHg. Then, IOP was increased in steps of 1 mmHg to 20 mmHg and decreased again. At each step, an optical coherence tomography volume scan was recorded. Displacements between subsequent scans were retrieved using a vector-based phase difference method. The induced corneal strain direction was determined by taking the axial gradient. In addition, corneal surface was detected and sagittal curvature maps computed.

Results: Corneal tissue presented a localized compressive strain in the direct vicinity of the stromal tunnel, which was independent on IOP change. The central and peripheral (exterior to the ICRS) cornea demonstrated compressive strains upon IOP increase, and tensile strains upon IOP decrease. ICRS induced an annular shaped tensile strain at its inner border, particularly during IOP increase. The compressive strains close to the tunnel remained after ICRS implantation. Corneal curvature changes were concentrated on regions where strain was induced.

Conclusions: ICRS implantation induces localized strains in the regions subjected to refractive changes, suggesting that corneal strain and curvature are directly related. Studying corneal strain in response to surgical intervention may provide new insights on underlying working principles.

Introduction:

Intracorneal ring segments (ICRS) have been developed as a tool for refractive correction in myopia[1], astigmatism[2] and especially corneal ectasias like keratoconus[3]. ICRS have been designed to selectively flatten the cornea and consequently achieve a refractive adjustment. Changes in corneal shape can be roughly predicted by the Barraquer thickness law[4]: in order to achieve a similar refractive outcome, either an equal amount of material could be theoretically removed from the central cornea or be added to the corneal periphery. In this sense, additive surgery like ICRS implantation is a technique of great potential as it permits a potentially permanent refractive correction without introducing a structural weakening, such as with laser ablation. Yet, the most important downside is that ICRS implantation remains poorly predictable. Commercially available ICRS are typically made of polymethylmethacrylate and are available in different dimensions with variations in thickness (150 to 350 μm), arc length (90 to 240°), optical zone (5 or 6 mm diameter), base width (600 to 800 μm) and cross-sectional shape (triangular, hexagonal, oval). Thicker rings with larger base width and small optical zone are considered to induce the highest correction[5], while long arc lengths (>180°) are rather used for myopic correction and short arc lengths for astigmatic corrections [6].

Clinical studies have mainly assessed geometrical and refractive changes associated with ICRS implantation[3,7] and accordingly nomograms were created. Such nomograms recommend ICRS dimension based on the location of the cone with regard to a reference meridian. It has also been suggested that the keratoconus phenotype visible on the refractive curvature map should be considered for ICRS geometrical design and selection.[8] Numerical studies have addressed ICRS implantation from a more theoretical perspective. Especially parametric analyses are

helpful to disentangle the effect of different geometric and surgical factors.[9–11] However, these models often overestimate the achieved outcome, possibly because the corneal material is not sufficiently well characterized, or because long-term post-surgical processes such as epithelial or corneal remodeling have not been accounted for.

We hypothesize that in order to better understand the underlying mechanisms of the ICRS-induced refractive change, it would be fundamental to quantify the stress and strain fields provoked by ICRS implantation. A recent numerical study evaluated the change in corneal stress distribution after ICRS implantation[9] and found that in the anterior stroma stress relaxed, while in the posterior stroma stress increased. Interestingly, the authors also showed that the ICRS implants were not able to stiffen the cornea globally. In the direct surrounding of the implant, stress was reported to have an uneven distribution, which was not further specified. Strain is the direct (deformation) response of the cornea to a stress field induced either physiologically through the intraocular pressure (IOP), or e.g. during refractive surgery. In an isotropic material, strain is linearly related to stress, but even in an anisotropic material like the cornea, the strain field is an important piece of information for mechanical characterization. To the best of our knowledge, the strain field induced in response to ICRS implantation has not been measured before.

Recently, we reported a novel technique[12,13] to visualize corneal strain based on optical coherence tomography (OCT) imaging and small-amplitude IOP modulation that permits an evaluation of corneal biomechanics in a condition very close to the eye's natural state. Applied to patterned corneal cross-linking,[14] this approach was able to detect a positive shift in strain limited to the irradiated (i.e. treated) area. While this information is not only relevant for a better understanding of involved

biomechanical processes in refractive treatments, it might also be an indicator of treatment success. The purpose of the current study was to experimentally quantify the axial strain field that is induced during ICRS implantation at different steps of the surgery.

Methods:

Implantation procedure

Freshly enucleated porcine eyes were obtained from the slaughterhouse and used within 8 hours. The ICRS investigated in here had a triangular cross-section, a thickness of 300 μm, an optical zone of 5 mm and did span over an arc length of 325° (Keraring, Mediphacos Belo Horizonte, Minas Gerais, Brazil). This geometry was chosen to guarantee a pronounced effect even in the porcine cornea, which is thicker than the human cornea (878 μm[15] vs 515 μm[16]) the ICRS was designed for. Furthermore, a large arc length was taken to maximize the induced strains. Tunnel creation was performed manually with dissectors dedicated for this purpose. The control conditions consisted of (i) a full (360°) corneal tunnel only and (ii) a virgin cornea.

Optical coherence elastography (OCE)

Imaging was conducted with a spectrometer based custom-built optical coherence tomography system described earlier.[12,14] Briefly, the system had an axial and lateral resolution of 3.9 and 12.4 μm in tissue, respectively. The intraocular pressure (IOP) was adjusted to 15 mmHg before the first measurement was taken. Subsequently, the IOP was increased in steps of 1 mmHg from 15 to 20 mmHg and back to 15 mmHg using a needle connected to a water column and a syringe. At each pressure step, a

volume scan consisting of 1000 x 100 A-scans spanning over an area of 10x10 mm was recorded. Large scale motion (more than 1 pixel) between two subsequently recorded volume scans was determined using a cross-correlation approach. Then axially induced corneal strain was determined by calculating the axial gradient (in direction of the OCT beam) of the phase difference between the two scans, following a vector-based phase approach described in more detail earlier.[12,14] In this context, axial compressive strains (meaning tissue compaction) can be observed during IOP increase and axial tensile strains (meaning tissue expansion / stretching) during IOP decrease. Our previous study demonstrated[12] adequate controls with similar post-mortem time are important when looking at comparisons of the strain profile. Therefore, we paid attention that the different conditions were measured in close temporal distance. Overall, the measurement of a single cornea took 5 min.

Curvature analysis

Surface detection of the anterior cornea was implemented by strongest reflection tracking starting from the apex. The mean surface corresponding to an IOP between 15 and 20 mmHg was used for subsequent analyses. Next, the highest point of the cornea was determined and corneal elevation centered on this point. Finally, sagittal radius of curvature was computed and converted into dioptric power using a corneal refractive index of 1.375.

Results:

Optical coherence elastography

Figure 1 presents the cross-sectional view of the corneal structure and axial strain during pressure increase and decrease. As expected, during pressure increase

corneas experienced compression resulting in negative axial strain and during pressure decrease corneas recovered resulting in positive axial strain. The virgin cornea demonstrated a homogenous strain distribution across the entire cornea (panel a). Manual tunnel creation alone did cause localized compressive axial strain above and below the cut (panel b), independent of pressure increase or decrease, while the central portion of the cornea showed a similar response as the virgin cornea.

Figure 2 presents corneal cross-sectional strain distribution after ICRS implantation at different locations of the cornea. In the periphery – outside of the ICRS – the tissue showed similar compressive and tensile behavior as the virgin cornea. In the direct vicinity of the corneal tunnel (panel a), the compressive strain was similar to the cornea with tunnel creation only. At the outer edge of the ICRS (panel b), during IOP increase the implant induced tensile strain located under the bottom corners, which got further enhanced during IOP decrease. Furthermore, compressive strain was induced at the peak of the ICRS, particularly during IOP increase. At approx. ¼ of the ICRS (panel c), the implant caused tensile strain in the anterior cornea, precisely coinciding with the region between the two arcs of the ICRS, both during IOP increase and decrease. Towards the center of the ICRS where the distance between the arcs were higher (panel d), the implant induced localized tensile strains, which were predominantly located in the posterior cornea. The central anterior cornea presented compressive strain during IOP increase, which however did not fully recover during IOP decrease.

Figure 3 shows the corresponding enface view of corneal structure and axial strain during pressure increase and decrease. The compressive strain in the vicinity of the tunnel is visible along its entire length. After ICRS implantation (panel c), during IOP increase a second ring of positive strain (red color) became visible at the inner edge of the ICRS, indicating a region of localized tissue relaxation. During IOP decrease

mostly positive strains were observed, hence localized relaxation due to ICRS implantation is visible with less contrast. Notably however, after ICRS implantation the strain amplitude in the center was higher than in virgin and tunnel-only controls. **Table 1** summarizes the axial strain distribution in the cornea observed with the different conditions.

Axial strain profile

Figure 4 presents the axial strain profile during IOP increase in the most central optical zone of 2 mm diameter as well as the corresponding axial displacement as a function of IOP. During IOP increase (panel a), central corneal strain in virgin and tunnel-only corneas were similar and tended to have small negative values (indicating compression) throughout the whole cornea. In contrast, corneas with an ICRS implanted presented a pronounced – yet not significant – positive axial strain (relaxation) in the posterior 20% of the tissue. During IOP decrease (panel b), corneal strain values were generally larger and had positive sign, except in the anterior 10% of the cornea where negative strains were observed. Similar to IOP increase, after ICRS implantation the posterior 20% of the cornea demonstrated significantly higher positive strain values than virgin or tunnel-only corneas (at 850μm depth: virgin vs ICRS, $p=0.003$; tunnel-only vs ICRS, $p=0.026$) indicating stronger posterior relaxation with ICRS. Axial displacement (panel c) was largest in the virgin cornea and smallest after ICRS implantation. Noticeably, the induced deformation during IOP modulation was mostly reversible in the cornea with ICRS, however all conditions demonstrated a hysteresis. Hysteresis in this context refers to the remaining deformation after IOP modulation, which was assessed the second time an IOP of 15 mmHg was reached (accumulated deformation in panel C).

Curvature analysis

Figure 5 presents the sagittal curvature map of the cornea before and after ICRS implantation. Tunnel creation alone (panel a) left corneal curvature unaffected (41.1±2.1 diopters), except for few localized aberrations. After ICRS implantation (panel b) a pronounced decrease in corneal curvature to 21.8±9.0 diopters was observed inside the ICRS implantation area, which went along with a ring of curvature increase to 53.5±8.9 diopters located in the periphery, outside of the ICRS implantation. Interestingly, the region that flattened most did match surprisingly well with the region in which localized strain alterations were observed, compare dashed reference circles in Figures 3 and 5.

Discussion:

We report for the first-time corneal strain alterations resulting from ICRS implantation measured under close-to-physiologic loading conditions. We demonstrate that localized corneal curvature changes are mostly restricted to the region in which corneal strain is induced. This observation is in line with previous literature suggesting that the regularizing effect of an ICRS on the cornea is attributed to local bulking rather than globalized stiffening.[9] The observed annular region of positive strain that was induced interior to the ICRS corresponds to the predicted relaxation of the anterior cornea in simulations[9]. The corneal strain profile demonstrated that in the central tissue posterior relaxation was even more dominant. Due to the positive sign of strains induced by the ICRS, differences were more apparent in OCT images during IOP increase (global stressing) than decrease (global relaxation). Overall, the location of ICRS-based strains matched well with the observed sagittal curvature changes suggesting that corneal strain amplitude and curvature were directly related. Interestingly, the induced displacement was more reversible after ICRS implantation.

This was likely a result of the ICRS reducing corneal strain by taking up part of the applied stress, which results in shifting the physiologic state towards the left (i.e. towards the linear elastic region) in the stress-strain diagram and reducing the risk of plastic deformation. In the end, these observations suggest that corneal tissue interior to a 325° arc length ICRS becomes protected from mechanical stress, which might be favorable for preventing keratoconus progression, if the implant is located close to the focal weakening. Since the distribution of stress may be potentially different when two segments of ICRS are implanted - instead of just one, as this study evaluated - this same hypothesis might not be interchangeable in such a situation. Further studies are needed to evaluate such a hypothesis.

Corneal tunnel creation alone did only cause few localized optical aberrations, which were likely associated with epithelial defects. The fact that compressive strains in the vicinity of the tunnel were independent of IOP increase or decrease indicates that these strains likely resulted from tissue insult during manual tunnel creation. Manual creation of corneal tunnel requires the use of a dissector that tears up the cornea along a lamellar plane by rotating the dissector. Due to this local application of brute force, it is reasonable to expect a longer lasting mechanical impact on neighboring tissue that even outlasts the measurement period of the current study.

Interestingly, the induced sagittal curvature changes observed after ICRS implantation were substantially higher (-19.3 diopters) than expected clinically (~ -6 diopters) for long-arc ICRS dimensions[17,18]. On one hand, this difference may be expected from the fact that refractive corrections after ICRS implantation decrease within the initial post-operative time. Assessment of the refractive state in clinical studies occurred as early as 1-day post-operative[19]. Follow-up after 3 months showed that refractive corrections became 13% less pronounced[19], suggesting that corneal stroma and

epithelium undergo important remodeling after surgery. On the other hand, this difference could be related to the fact that tunnel depth was slightly shallower (56 to 64%) in the current study than recommended in patients (70% to 75%). A numerical study[10] suggests that a more shallow implantation depth provokes a larger reduction of spherical equivalent. An additional interesting point observed here was the compressive strain induced at the outer edge of the ICRS, particularly during the IOP increase. Clinically, such a compressive force could explain late extrusions and recurrent epithelial erosions observed in cases where the rings are superficially implanted.

This study is not exempt of limitations. First of all, the stromal tunnel was created manually without access to a surgical microscope, which made it challenging to achieve an appropriate tunnel depth and avoid corneal penetration. However, corneas that had perforation were naturally excluded from this analysis. Second, the resulting limited number of eyes that were successfully implanted and measured. Third, the fact that healthy porcine eyes were investigated. Porcine corneas are reportedly[15,16] thicker than human corneas (factor ~1.7). The difference is even more pronounced when considering ectatic (e.g. keratoconic) human corneas, in which thickness is locally reduced and in which ICRS are typically implanted. Therefore, the strain amplitude and strain pattern observed in the current study may result noticeably different in those corneas. Future research is demanded to overcome these issues and to quantify the induced strain field with different ICRS dimensions, arc lengths and depths of corneal implantation, as well as in a disease model of corneal ectasia.

In conclusion, the current study proves the usefulness of OCE for the assessment of the spatially highly-resolved strain field induced by additive surgery such as ICRS implantation. In particular, we demonstrated that the corneal curvature map and the

axial strain field are directly related, which might open a new way to better understand and predict the underlying mechanisms of ICRS surgery.

Acknowledgement:

This study received funding from the Swiss National Science Foundation (Ambizione PZ00P2_174113 to SK). The authors thank Mediphacos (Belo Horizonte, MG, Brasil) for sponsoring the intrastromal ring segments and the surgical kit required for implantation.

References:

1. Schanzlin, D. J., Asbell, P. A., Burris, T. E. & Durrie, D. S. The Intrastromal Corneal Ring Segments: Phase II Results far the Correction of Myopia. *Ophthalmology* **104**, 1067–1078 (1997).
2. Arriola-Villalobos, P. *et al.* Intrastromal corneal ring segment implantation for high astigmatism after penetrating keratoplasty. *J. Cataract Refract. Surg.* **35**, 1878–1884 (2009).
3. Miranda, D. *et al. Ferrara intrastromal corneal ring segments for severe keratoconus*. (Slack Incorporated Thorofare, NJ, 2003).
4. Barraquer, J. I. Modification of refraction by means of intracorneal inclusions. *Int. Ophthalmol. Clin.* **6**, 53–78 (1966).
5. Giacomin, N. T. *et al.* Intracorneal ring segments implantation for corneal ectasia. *J. Refract. Surg.* **32**, 829–839 (2016).
6. Ruckhofer, J., Stoiber, J., Twa, M. D. & ünther Grabner, G. Correction of astigmatism with short arc-length intrastromal corneal ring segments: preliminary results. *Ophthalmology* **110**, 516–524 (2003).
7. Kubaloglu, A. *et al.* Intrastromal corneal ring segment implantation for the treatment of keratoconus. *Cornea* **30**, 11–17 (2011).
8. Fernández-Vega Cueto, L. *et al.* Intrastromal corneal ring segment implantation in 409 paracentral keratoconic eyes. *Cornea* **35**, 1421–1426 (2016).
9. Ariza-Gracia, M. Á., Flecha-Lescún, J., Büchler, P. & Calvo, B. Corneal biomechanics after intrastromal ring surgery: Optomechanical in silico assessment. *Transl. Vis. Sci. Technol.* **9**, 26–26 (2020).

10. Ariza-Gracia, M. A., Flecha-Lescún, J., Calzada, B. C. & Büchler, P. Biomechanically-driven simulations of the MyoRing treatment in subjects with high myopia. *Invest. Ophthalmol. Vis. Sci.* **61**, 4722–4722 (2020).
11. Kling, S. & Marcos, S. Finite-element modeling of intrastromal ring segment implantation into a hyperelastic cornea. *Invest. Ophthalmol. Vis. Sci.* **54**, 881–889 (2013).
12. Kling, S., Khodadadi, H. & Goksel, O. Optical Coherence Elastography-Based Corneal Strain Imaging During Low-Amplitude Intraocular Pressure Modulation. *Front. Bioeng. Biotechnol.* **7**, (2019).
13. Kling, S., Torres-Netto, E. A., Spiru, B., Sekundo, W. & Hafezi, F. Quasi-static optical coherence elastography to characterize human corneal biomechanical properties. *Invest. Ophthalmol. Vis. Sci.* **61**, 29–29 (2020).
14. Kling, S. Optical coherence elastography by ambient pressure modulation for high-resolution strain mapping applied to patterned cross-linking. *J. R. Soc. Interface* **17**, 20190786 (2020).
15. Sanchez, I., Martin, R., Ussa, F. & Fernandez-Bueno, I. The parameters of the porcine eyeball. *Graefes Arch. Clin. Exp. Ophthalmol.* **249**, 475–482 (2011).
16. OLSEN, T. & EHLERS, N. The thickness of the human cornea as determined by a specular method. *Acta Ophthalmol. (Copenh.)* **62**, 859–871 (1984).
17. Izquierdo Jr, L., Rodríguez, A. M., Sarquis, R. A., Altamirano, D. & Henriquez, M. A. Intracorneal circular ring implant with femtosecond laser: Pocket versus tunnel. *Eur. J. Ophthalmol.* 1120672121994729 (2021).
18. Sadoughi, M. M. *et al.* Femtosecond laser implantation of a 340-degree intrastromal corneal ring segment in keratoconus: short-term outcomes. *J. Cataract Refract. Surg.* **43**, 1251–1256 (2017).

19. Michael, R. *et al.* Refractive and biomechanical changes with intrastromal ring segments for keratoconus. *Acta Ophthalmol. Scand.* **85**, (2007).

Figures:

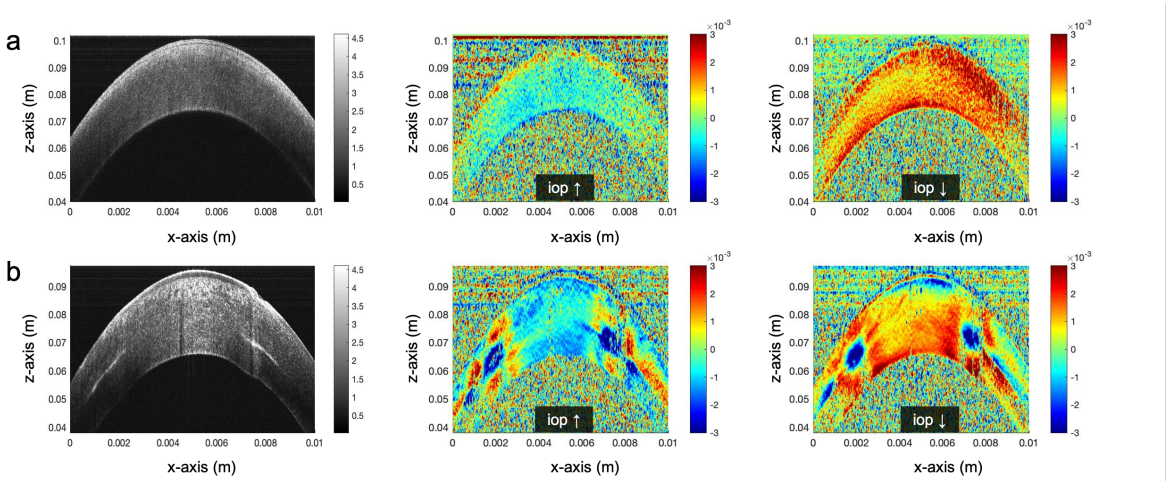

Figure 1. Cross-sectional view of standard structural imaging (left panel) and strain imaging (a) in a virgin cornea, (b) after tunnel creation, during IOP increase (middle panel) and IOP decrease (right panel). Red color means positive axial strain (i.e. relaxation), blue color means negative axial strain (i.e. compression). Predominantly, axial compressive strains are observed during IOP increase and axial tensile strains during IOP decrease. After tunnel creation, localized compressive strains occurred in the direct vicinity of the tunnel.

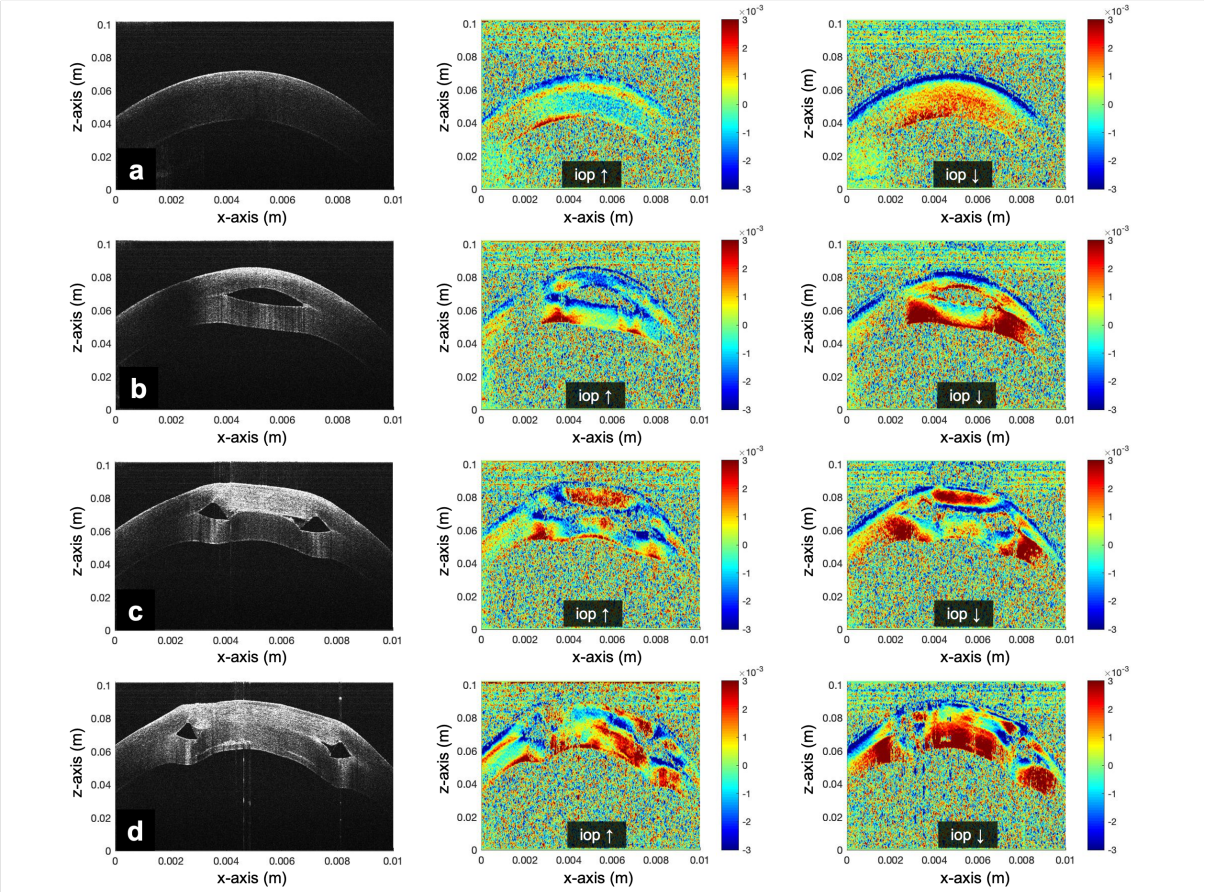

Figure 2. Cross-sectional view with standard structural imaging (left panel) and strain imaging after ICRS (300μm thickness, arc length 325°) implantation at different

locations of the cornea from periphery (top line) to center (bottom line), during IOP increase (middle panel) and IOP decrease (right panel). Red color means positive axial strain (i.e. relaxation), blue color means negative axial strain (i.e. compression). The panels a-d represent different locations on the cornea: at direct vicinity of the corneal tunnel (panel a), the outer edge of the ICRS (panel b), at approx. ¼ of the ICRS (panel c) and at a higher distance between arcs (panel d).ICRS implantation introduced tensile strains located in the anterior cornea at the inner edge of the segment, but hardly affected tissue strains in the periphery of the segment. The implant also induced some localized strains in its direct vicinity.

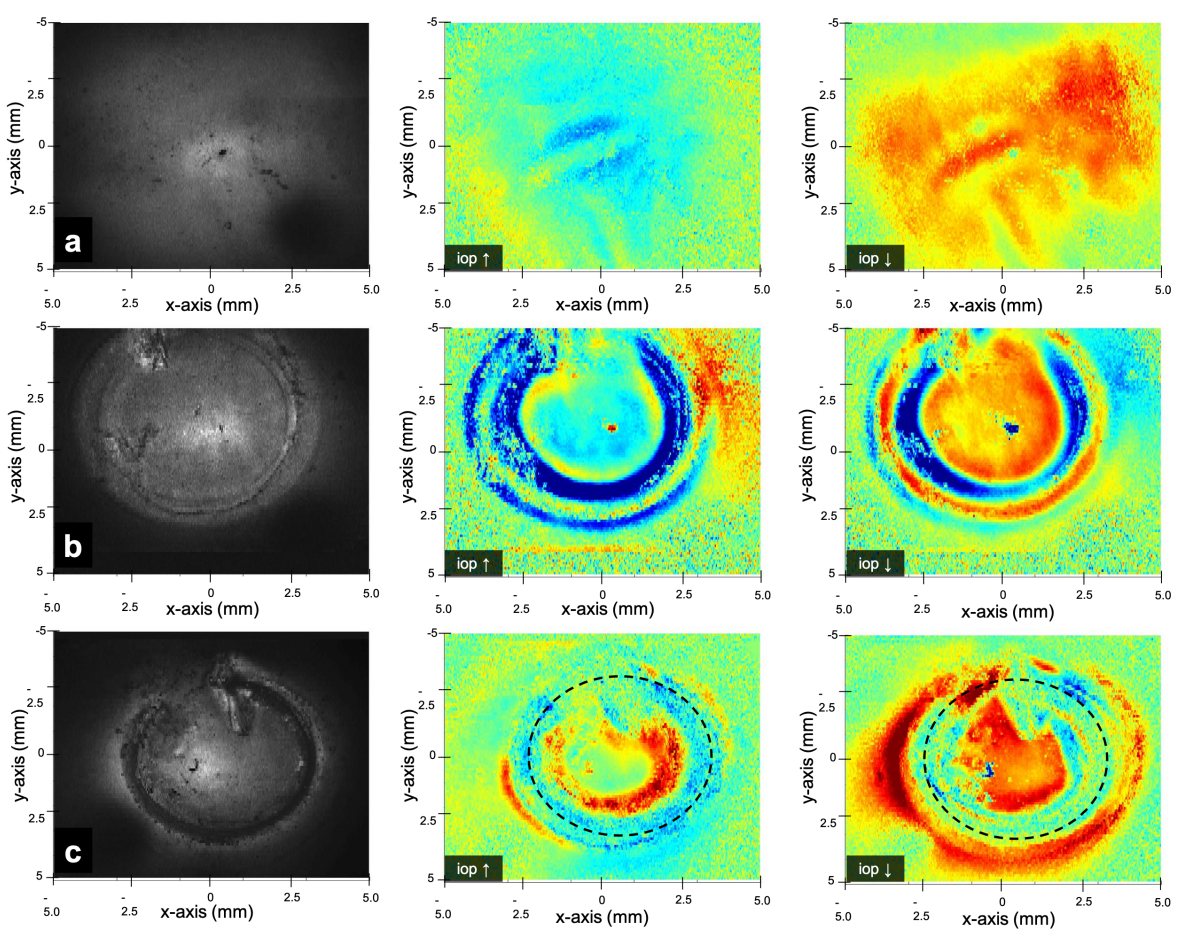

Figure 3. Enface view with standard structural imaging (left panel) and strain imaging in (a) a virgin cornea, (b) after tunnel creation, (c) after ICRS (300μm thickness, arc length 325°) implantation, during IOP increase (middle panel) and IOP decrease (right panel). Dashed circles are a reference for comparison with Figure 5. Red color means relaxation, blue color means compression. After ICRS implantation a second ring of positive strain (red color) was observed at the inner edge of the ICRS, indicating localized tissue relaxation.

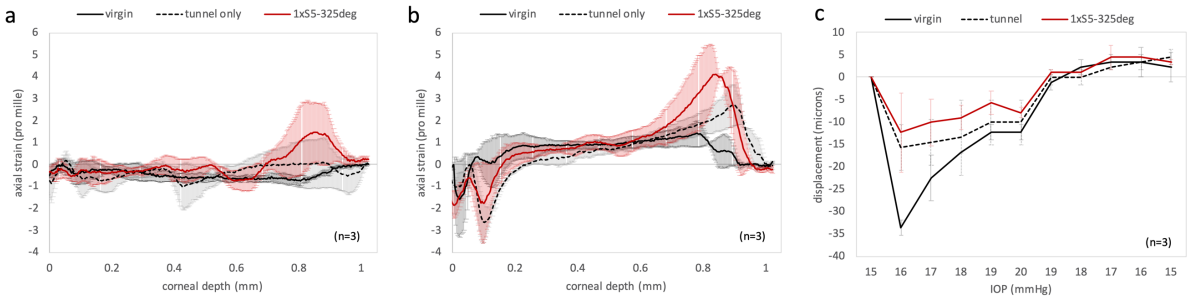

Figure 4. Axial strain profile in the central optical zone of 4mm diameter. (**A**) During IOP increase. Without an ICRS, strain amplitudes are mostly small and of compressive nature. With an ICRS, a trend towards tissue relaxation in the posterior cornea is observed. (**B**) During IOP decrease. Generally larger strain amplitudes are observed. With an ICRS, the posterior cornea demonstrated a significantly increased tissue relaxation. (**C**) Axial displacement. With an ICRS, the smallest displacement was observed.

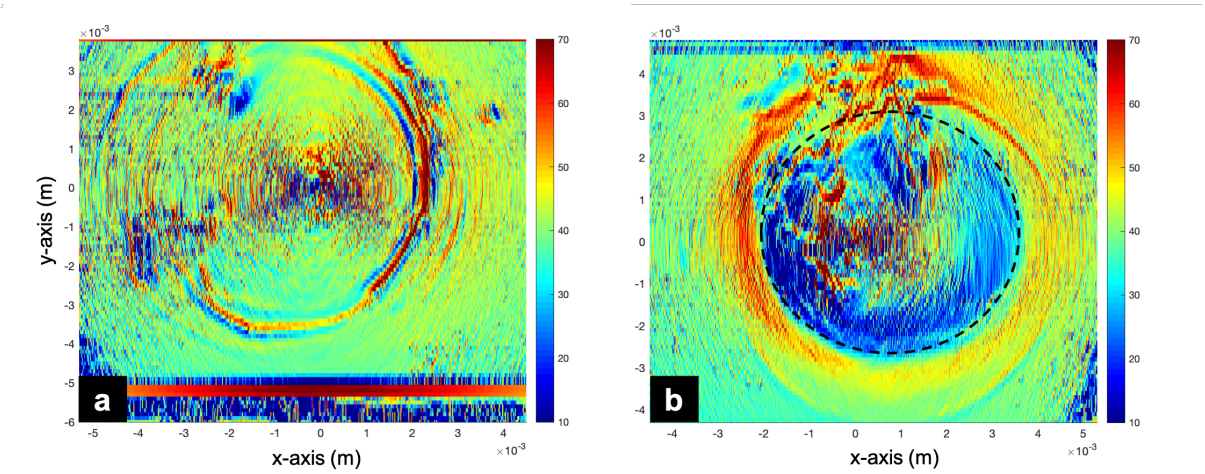

Figure 5. Sagittal curvature map of the cornea with (**A**) tunnel creation only, (**B**) ICRS implantation. The dashed circle is a reference for comparison with Figure 3. Substantial corneal flattening was observed interior to the ICRS and localized corneal steepening in the direct periphery of the ICRS.

Table 1. Overview of axial strain in the 80% anterior and 20% posterior corneal stroma, both during IOP increase and decrease. Central refers to the region interior (i.e. the optical zone) of the ICRS. comp. = compressive (negative) strains; relax. = tensile (positive) strains

		IOP↑		IOP↓	
		central	periphery	central	periphery
virgin	ant	comp.		relax.	
	post	comp.		relax.	
	ant	comp.	comp.	relax.	relax.

tunnel-only	post	comp.	comp.	relax.	relax.
ICRS	ant	comp.	comp.	relax.	relax.
	post	**relax.**	comp.	**relax.↑**	relax.